NANO LETTERS

Letter

pubs.acs.org/NanoLett

Strong Enhancement of Light–Matter Interaction in Graphene Coupled to a Photonic Crystal Nanocavity

Xuetao Gan,[†,‡] Kin Fai Mak,[§] Yuanda Gao,[∥] Yumeng You,[§] Fariba Hatami,[⊥] James Hone,[∥] Tony F. Heinz,[†,§] and Dirk Englund*[,†,#]

[†]Department of Electrical Engineering, Columbia University, New York, New York 10027, United States

[‡]School of Science, Northwestern Polytechnical University, Xi'an 710072, China

[§]Department of Physics, Columbia University, New York, New York 10027, United States

[∥]Department of Mechanical Engineering, Columbia University, New York, New York 10027, United States

[⊥]Department of Physics, Humboldt-Universität zu Berlin, Newtonstrasse 15, 12489 Berlin, Germany

[#]Department of Applied Physics and Applied Mathematics, Columbia University, New York, New York 10027, United States

Supporting Information

ABSTRACT: We demonstrate a large enhancement in the interaction of light with graphene through coupling with localized modes in a photonic crystal nanocavity. Spectroscopic studies show that a single atomic layer of graphene reduces the cavity reflection by more than a factor of one hundred, while also sharply reducing the cavity quality factor. The strong interaction allows for cavity-enhanced Raman spectroscopy on subwavelength regions of a graphene sample. A coupled-mode theory model matches experimental observations and indicates significantly increased light absorption in the graphene layer. The coupled graphene–cavity system also enables precise measurements of graphene's complex refractive index.

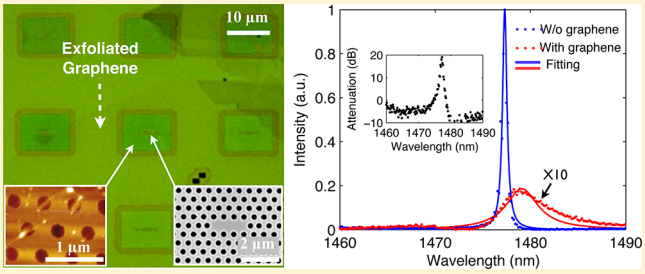

KEYWORDS: *Graphene, photonic crystal cavity, optoelectronics, Raman spectroscopy*

Graphene, a single atomic layer of graphite, possesses unique electronic properties that have led to a range of promising optoelectronic devices,[1] such as photodetectors,[2−5] tunable broadband modulators,[6,7] saturable absorbers,[8,9] and nonlinear media for four-wave mixing.[10−12] Although the optical absorption of graphene is high given its single atom thickness,[13,14] it is low in absolute terms, with an absorbance of approximately 2.3% in the near-infrared and visible regions. A much stronger absorption is needed for many electro-optic and all-optical applications. The absorption, and generally the light–graphene interaction, has been increased using a variety of techniques, including surface plasmon polariton states providing subwavelength confinement,[15−20] guided modes in silicon waveguides enabling 5 dB optical attenuation over a 40 μm channel length,[6,7] and distributed Bragg reflector microcavities enhancing light absorption 26 times.[21]

Here, we describe a dramatic enhancement of the light–matter interaction in graphene using light captured in a subwavelength nanocavity in a planar photonic crystal (PPC). This strong coupling of graphene to the PPC cavity reduces the cavity reflection by more than 100 times. We explain our observations using a coupled mode theory, which indicates that the graphene–cavity system enables greater than 45% light absorption under optimized conditions. These results open a route to strong coupling of electromagnetic fields to single-layer graphene and to a new generation of compact graphene photonic devices. The enhancement of the electromagnetic fields provided by PPC nanocavities can also be applied to the spectroscopy of graphene. In particular, we show that the nanocavity allows for a precise determination of the complex refraction index of graphene, as well as cavity-enhanced Raman scattering with excitation localized to a subwavelength region.

When an optical field couples into a mode of an optical cavity, its intensity is increased in proportion with the mode's Q/V_{mode} ratio of quality (Q) factor to mode volume (V_{mode}). PPC nanocavities, which display an extremely high Q factor (up to 10^6) and ultrasmall V_{mode} (on the order of a cubic wavelength), can therefore amplify the intensity of the incident light by many orders of magnitude. Here, we employ linear three-hole defect cavities (L3)[22] in air-suspended two-dimensional PPCs. These structures were fabricated by a combination of electron beam lithography and dry/wet etching steps in a 138 nm thick gallium phosphide (GaP) membrane (see Supporting Information). We prepared single-layer graphene by mechanical exfoliation and chemical vapor deposition (CVD); the exfoliated and CVD-grown graphene samples

Received: July 24, 2012
Revised: October 5, 2012
Published: October 8, 2012

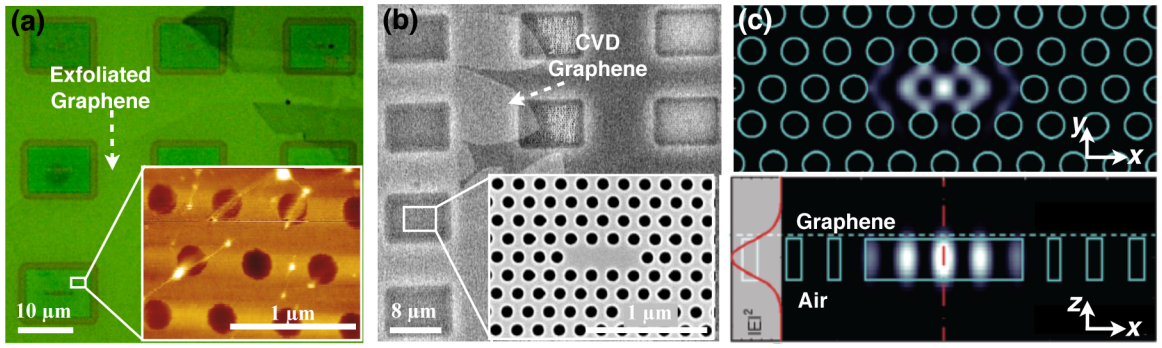

Figure 1. Planar photonic crystal cavities integrated with graphene. (a) Optical microscope image of the PPC cavities integrated with exfoliated graphene. The inset shows an atomic force microscope image of the device. (b) Scanning electron microscope image of the PPC cavities integrated with CVD graphene. The flower shapes define the edges of the graphene monolayer. (c) Simulated energy distribution of fundamental resonant mode of the L3 cavity, shown in plane (top) and in cross-section (bottom). The graphene layer interacts with the evanescent field.

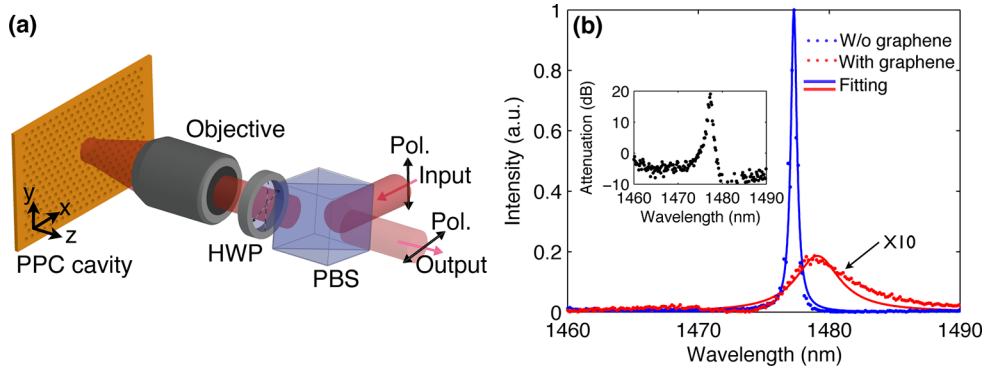

Figure 2. (a) Schematic of the cross-polarization confocal microscope, where the black double-arrowed lines represent the polarization directions. HWP: half-wave plate, PBS: polarized beam splitter. (b) Reflection spectra of the PPC cavity before and after the deposition of an exfoliated graphene monolayer (magnified 10 times). Inset: Spectrum of the relative attenuation of the cavity with graphene compared to the same cavity without graphene. At the peak of reflection of the unloaded cavity, the attenuation increases by 20 dB by inserting a single layer of graphene.

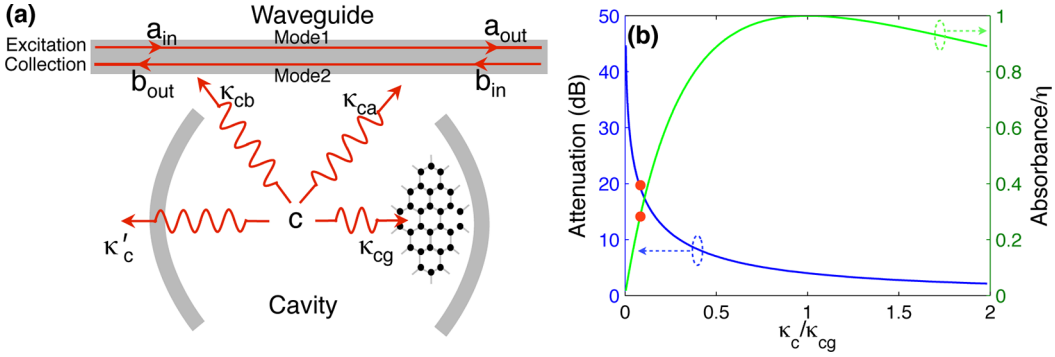

Figure 3. (a) Schematic of the coupled graphene−cavity model. The cavity integrated with graphene is forward and backward coupled with Mode 1 and Mode 2, respectively. The total energy decay rate of the unloaded cavity κ_c consists of the forward and backward coupling rates κ_{ca} and κ_{cb}, respectively, into the waveguide modes, and the decay rate κ_c' due to other lossy modes and material absorption. The decay rate κ_{cg} arises from the absorption of the graphene layer. (b) The calculated relative attenuation for the cavity loaded with graphene and the empty cavity (left scale) and the calculated graphene absorbance (right scale) for the graphene−cavity system versus the ratio of the cavity decay rates κ_c/κ_{cg}. The relative attenuation is calculated at the frequency of the unloaded cavity resonance, while the graphene absorbance is calculated for excitation at the frequency of the loaded cavity. The red dots are the measured values for the device in Figure 2, shown in the figure for a ratio of $\kappa_c/\kappa_{cg} \approx 0.15$.

were transferred onto the PPC nanocavities by a precision transfer technique[23] and a dry transfer technique,[24] respectively.

The optical microscope image in Figure 1a shows several cavities covered by exfoliated graphene, including in the inset an atomic force microscope image of a graphene layer suspended over the air-holes. The scanning electron microscope (SEM) image in Figure 1b shows devices covered by CVD-grown graphene. The graphene layer interacts with the cavity through the evanescent field above the subwavelength membrane, as shown in Figure 1c. By choosing the thickness of the membrane between $d = 0.29a$ to $0.65a$, where a is the PPC lattice spacing, we can control the magnitude of the evanescent electric field amplitude ($E_{graphene}$) at the graphene location to be between 10% and 40% of the field maximum (E_{max}) at the center of the structures.

dx.doi.org/10.1021/nl302746n | Nano Lett. 2012, 12, 5626−5631

We characterize the graphene-cavity devices using a cross-polarization confocal microscope with a broad-band (supercontinuum laser) excitation source, as shown in Figure 2a. The input field is polarized at 45° to the linearly polarized cavity mode, and the collected reflection field is polarized at −45° to the cavity mode.[25] A half-wave plate enables us to rotate the input and output polarizations to achieve an arbitrary orientation with respect to the cavity axis.

Figure 2b displays the measured reflectivity of the cavity shown in Figure 1a, which has a lattice spacing of a = 480 nm and a hole radius of $r = 0.24a$. The blue dotted line represents the reflectivity spectrum (R_0) of the unloaded cavity (before graphene deposition) as recorded with a spectrometer having a resolution of 0.05 nm. The fundamental mode resonance occurs at 1477.3 nm and has a Q factor of 2640, as estimated by fitting to a Lorentzian line shape. After the transfer of a graphene monolayer, the cavity reflection spectrum (R_g) indicates that the Q factor drops sharply to 360, while the resonance is red-shifted by 1.8 nm, as shown by the red dotted line in Figure 2b. Remarkably, the graphene layer renders the cavity nearly opaque: the relative cavity attenuation, defined as $[-10\log_{10}(R_g/R_0)]$, increases by 20 dB at the resonance of the unloaded cavity at 1477.3 nm. The full spectrally resolved relative attenuation is shown in the inset of Figure 2b; it is asymmetric and includes a region of negative relative attenuation because of the red-shift of the cavity resonance.

To explain these experimental observations, we model the graphene−cavity system by coupled mode theory (see Supporting Information), as shown schematically in Figure 3a. The cavity integrated with graphene couples with a waveguide through the forward and backward propagating modes, Mode 1 and Mode 2, at rates of κ_{ca} and κ_{cb}, respectively. The model ignores the cavity loss arising from the GaP bulk absorption since this semiconductor has a large indirect bandgap (~2.26 eV) and an absorption coefficient below 1 cm^{-1}.[26] The loss of the unloaded cavity is caused by out-of-plane radiation with an energy decay rate of $\kappa_c = \omega_0/Q$, where ω_0 is the angular frequency of the cavity resonance. The deposition of the graphene layer causes an additional cavity loss characterized by an energy decay rate κ_{cg}, together with a frequency shift $\Delta\omega$ in the cavity resonance. Since the graphene layer is very thin, we neglect any scattering loss of the cavity caused by the graphene deposition, as verified using finite difference time domain (FDTD) simulations with a small planar perturbation of the cavity to model the graphene sheet.

For the cross-polarization confocal microscope, the excitation mode (Mode 1) $\mathbf{a}_{in}$ and collected mode (Mode 2) $\mathbf{b}_{out}$ are approximately Gaussian spatial modes, given by the optics of the confocal microscope. Due to the symmetric confinement, the resonant mode of the PPC cavity decays equally into the forward and backward propagating waveguide modes. We assume a coupling efficiency η between the microscope modes and the cavity radiation field, so that the cavity mode couples with the microscope modes with rates $\kappa_{ca} = \kappa_{cb} = \eta\kappa_c$. The steady-state solution to the coupled mode equations then yields frequency-dependent reflection $R_g(\omega)$ and absorption $A_g(\omega)$ coefficients of the loaded cavity:

$$R_g(\omega) = \frac{\eta^2\kappa_c^2}{(\omega_0 + \Delta\omega - \omega)^2 + (\kappa_c/2 + \kappa_{cg}/2)^2} \quad (1)$$

$$A_g(\omega) = \frac{\eta\kappa_c\kappa_{cg}}{(\omega_0 + \Delta\omega - \omega)^2 + (\kappa_c/2 + \kappa_{cg}/2)^2} \quad (2)$$

The same expressions apply for the unloaded cavity reflection $R_0(\omega)$ and absorption $A_0(\omega)$ coefficients, but with κ_{cg} and $\Delta\omega$ set to zero. Fitting the experimental reflection spectra (Figure 2b) to eq 1, we obtain $\omega_0 = 1.28 \times 10^3$ THz, $\kappa_c = 1.9 \times 10^{-4}\omega_0$, $\Delta\omega = -1.24 \times 10^{-3}(1 \pm 0.016)\omega_0$, and $\kappa_{cg} = 2.4 \times 10^{-3}(1 \pm 0.016)\omega_0$, where the estimated uncertainties are near those expected for shot noise from our cooled CCD camera. The resonance frequency shift $\Delta\omega$ and additional energy decay rate κ_{cg} are comparable in magnitude and are much higher than κ_c. This shows that the graphene layer dominates the photon loss with a factor of $\kappa_{cg}/(\kappa_{cg} + \kappa_c) \approx 92\%$ inside the nanocavity.

We confirm the strong perturbation of graphene on the cavity from a numerical simulation of the field−graphene interaction, which enables us to deduce the graphene's complex dielectric constant. The unloaded cavity's energy density is shown in Figure 1c, as obtained from a three-dimensional FDTD simulation that yields the complex resonant field $\mathbf{E}(\mathbf{r})$. The same simulation yields a cavity quality factor Q = 7600, which is lower than the optimal value of 45 000[22] due to the thinness of the GaP slab. The graphene layer has an anisotropic complex dielectric function with in-plane and perpendicular components given by $(\varepsilon_{g1\parallel} + i\varepsilon_{g2\parallel})$ and $(\varepsilon_{g1\perp} + i\varepsilon_{g2\perp})$, where $\varepsilon_{g2\perp} \approx 0$ for near-infrared radiation.[27] Using the anisotropic perturbation theory,[28] we can now estimate the graphene absorption rate as $\kappa_{cg} = \omega_0[(\int d^3\mathbf{r}\varepsilon_{g2\parallel}(\mathbf{r})|\mathbf{E}_\parallel(\mathbf{r})|^2)/(\int d^3\mathbf{r}\varepsilon_s(\mathbf{r})|\mathbf{E}(\mathbf{r})|^2)]$ and the cavity frequency shift as $\Delta\omega = -(1/2)\omega_0[\int d^3\mathbf{r}((\varepsilon_{g1\parallel}(\mathbf{r}) - 1)|\mathbf{E}_\parallel(\mathbf{r})|^2 + (\varepsilon_{g1\perp}(\mathbf{r}) - 1)|\mathbf{E}_\perp(\mathbf{r})|^2)]/(\int d^3\mathbf{r}\varepsilon_s(\mathbf{r})|\mathbf{E}(\mathbf{r})|^2)$. Here, $\mathbf{E}_\parallel(\mathbf{r})$ and $\mathbf{E}_\perp(\mathbf{r})$ are the in-plane and perpendicular components of $\mathbf{E}(\mathbf{r})$, and ε_s = 9.36 denotes the dielectric constant of the GaP substrate near ω_0. The measured rate $\kappa_{cg} = 2.4 \times 10^{-3}(1 \pm 0.016)\omega_0$ then yields a value for the imaginary part of graphene's dielectric function around the probe wavelength of 1480 nm of $\varepsilon_{g2\parallel} = 4.61 \pm 0.07$. This result is close to the previously reported value of $\varepsilon_{g2\parallel} = 4.62$ for graphene on a quartz substrate.[27] Note that the value of the dielectric function is quoted with the understanding that the graphene layer is treated as a homogeneous slab of a thickness of 0.34 nm, corresponding to the interlayer space in bulk graphite. Deducing the real part of graphene's dielectric constant from the measured $\Delta\omega$ is difficult due to the presence of two nonzero components $\varepsilon_{g1\parallel}$ and $\varepsilon_{g1\perp}$; in future studies, this measurement could be accomplished by employing a multi-mode cavity that provides multiple independent in-plane and perpendicular components of each resonant mode to resolve $\varepsilon_{g1\parallel}$ and $\varepsilon_{g1\perp}$. Here, on the other hand, we use the reported values of $\varepsilon_{g1\parallel} = 4.64$ and $\varepsilon_{g1\perp} = 2.79$ to verify our measured $\Delta\omega$.[27] Combining these values with the simulation of $\mathbf{E}(\mathbf{r})$, we predict $\Delta\omega = -1.22 \times 10^{-3}\omega_0$, in good agreement with our measurement.

The ability of the graphene−cavity system to control the cavity resonance and enhance absorption promises to substantially improve graphene-based optical devices, such as modulators and photodetectors. In this regard, it is useful to estimate the expected reflection attenuation and absorption as a function of the intrinsic cavity loss rate κ_c, the waveguide coupling efficiency η, and the graphene loss rate κ_{cg}. Based on the theoretical model of eqs 1 and 2, which adequately describes our experimental observations, we plot in Figure 3b the predicted value for the relative cavity attenuation, $-10\log_{10}(R_g/R_0)$, induced by the presence of graphene as a function

dx.doi.org/10.1021/nl302746n | Nano Lett. 2012, 12, 5626−5631

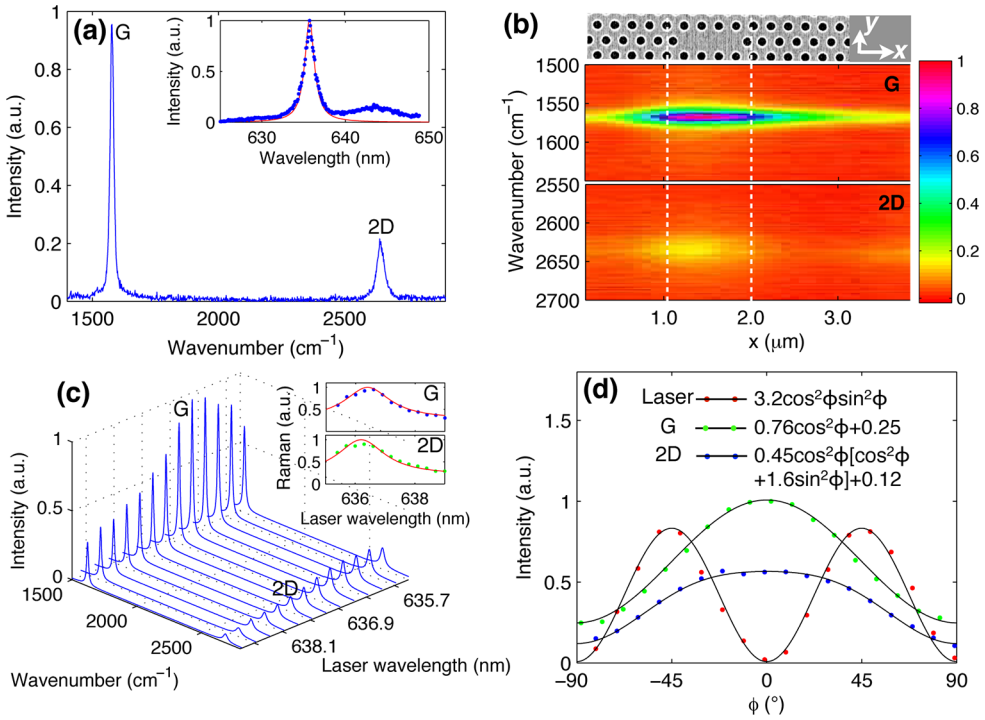

Figure 4. Enhanced Raman scattering from a graphene–cavity device. (a) Raman spectrum excited at 637 nm, showing the G and 2D bands. The inset displays the cavity resonance at 636.3 nm. (b) Spatial dependence of the cavity-enhanced Raman scattering process, displaying strong scattering when illuminated near the cavity defect region (indicated by the top SEM image). (c) Laser wavelength dependences of the Raman scattering. The dependence of the scattering intensities of the two modes on the excitation wavelength (inset) matches the response of the cavity resonance. (d) Polarization dependence of cavity-enhanced Raman signal, showing 90°-periodicity of the laser reflection and 180°-periodicity of the Raman peaks. The experimental results are fit well to a model accounting for the polarization of the cavity resonance and of the Raman response. The corresponding functional forms are indicated, including a contribution from the background signal not coupled through the cavity resonance.

of the ratio of the loss rate of the unloaded cavity to that for graphene, κ_c/κ_{cg}. For a cavity with high Q, we see that the added attenuation from a single layer of graphene can be as high as 40 dB (at the frequency of the original resonance). A modulation of this magnitude should be possible with existing PPC cavities ($Q \sim 10^6$). Even when $\kappa_c \approx \kappa_{cg}$, the reflection still drops by about 5 dB.

The absorption into graphene at the cavity resonance, $(\eta\kappa_c\kappa_{cg})/((\kappa_c/2 + \kappa_{cg}/2)^2)$, reaches its maximum value of η when $\kappa_c = \kappa_{cg}$, as shown in the green curve in Figure 3b. The condition for maximum absorption can be understood as follows: if $\kappa_c > \kappa_{cg}$, photons decay from the cavity before being absorbed by the graphene layer; alternatively, if $\kappa_c < \kappa_{cg}$, photons are not efficiently coupled into the cavity in the first place. For efficient absorption, the above equations show a linear dependence on η. This coupling efficiency can exceed 45% using on-chip side-coupling into the cavity from a waveguide[29] or tapered fiber coupling.[30] By employing efficient coupling and choosing $\kappa_c \sim \kappa_{cg}$, the model indicates that it is possible to reach 45% absorption into a monolayer of graphene, which can be improved further by placing a reflector under the cavity.[25]

As an immediate application of the enhanced graphene–light interaction in the PPC nanocavity, we consider now how the process of Raman scattering is modified via the cavity field enhancement. We use a different GaP PPC cavity with the fundamental mode at a shorter wavelength of 636.3 nm (inset of Figure 4a), ensuring that the Raman-scattered signal is still in the near-infrared for convenient detection. This device is coupled to a CVD-grown graphene layer and then yields a resonance with a Q-factor of about 330 (see Supporting Information). Figure 4a shows the Raman spectrum of graphene excited at 637 nm. We see prominent features at Raman shifts of 1578 cm^{-1} and 2640 cm^{-1} corresponding, respectively, to the well-known G and 2D bands. The 2D peak is weaker than the G peak because of the high doping level of the CVD-grown graphene,[31] as confirmed independently by conventional Raman measurements. Figure 4b demonstrates the cavity enhancement: when we spatially scan the device along the x-axis of the PPC, the Raman scattering is enhanced dramatically when pumped through the nanocavity defect. We verify the effect of the cavity-enhanced pump by sweeping the laser wavelength from 635 to 639 nm, covering the graphene–cavity resonance. Figure 4c shows the enhancement in the Raman scattering intensity for resonant excitation of the graphene–cavity. The wavelength dependence of both the G and 2D bands, plotted in the inset of Figure 4c, is accurately fit by a Lorentzian function centered at 636.3 nm with a Q factor of 330, consistent with the cavity resonance. In these measurements, the flat baseline arises from incident radiation that excites the graphene directly, not through the cavity mode. Normalizing the peak Raman signals to the baseline, we obtain a 2.8- and a 3.3-fold increase of the G and 2D bands, respectively. This wavelength dependence matches the expected cavity-field enhancement, which also increases absorption, with an enhancement factor of 3.41 (see Supporting Information).

The cavity-enhanced Raman scattering process can resolve the polarization dependence of the G and 2D bands. In this measurement, we use the half-wave plate before the microscope

dx.doi.org/10.1021/nl302746n | Nano Lett. 2012, 12, 5626–5631

objective rotate both direction of the orthogonal excitation and detection polarizations. In Figure 4d we plot these intensities against the angle ϕ between the input polarization and the axis of the cavity. The pump laser has a 90°-periodicity because it couples with an efficiency $\propto\cos^2\phi$ into the cavity excitation mode and with an efficiency $\propto\sin^2\phi$ into the collection mode. The G band scattering is seen to follow to a $\cos^2\phi$ variation, corresponding to the cavity input coupling efficiency and indicating the expected unpolarized character of the G-band Raman emission.[32] However, the 2D band scattering process is described by an anisotropic Raman tensor,[32] which leads to the more complicated polarization dependence displayed in Figure 4d. Using a simulation of the cavity field, we deduce that the ratio of the strength of the parallel to perpendicular emission for the Raman 2D band is 6.47 (see Supporting Information). Thus, the cavity not only enables us to enhance the Raman scattering efficiency, but also to determine the material's polarization dependence over a region of subwavelength spatial extent defined by the cavity mode.

In conclusion, we have demonstrated that the interaction of light with graphene can be greatly enhanced by coupling to a PPC nanocavity. We observe a 20 dB attenuation in the cavity reflection induced by a single layer of graphene. The experiments are modeled accurately by a coupled mode theory, which indicates that controlling this reflection could enable high-visibility modulators by electrical gating of the graphene sheet. Our observations and theoretical model predicts that, if the PPC cavities were designed with lower intrinsic Q (higher κ_c) or fabricated on thicker slab (lower κ_{cg}) to satisfy $\kappa_c = \kappa_{cg}$, then the absorption of light by a graphene monolayer could be improved to a maximum defined by the cavity coupling efficiency η. This indicates that absorption greater than 45% into graphene should be possible using efficient coupling strategies, such as tapered fiber or on-chip waveguide couplers.[29,30] By incorporating graphene into a cavity with traveling-wave resonant modes, such as a ring resonator, one should be able to achieve optical absorption by a single layer of graphene of 90%.[33] The cavity-enhanced optical absorption opens the door to promising applications of graphene as the active material in compact photodetectors, modulators, and other novel opto-electronic devices that combine the exceptional optical and electronic properties of graphene. The cavity-enhanced Raman scattering demonstrated in this paper could also serve as a precise tool for fundamental graphene studies; for instance, high-precision Raman scattering could aid in optical studies of grain boundaries and edge states.[34] Such studies could exploit the high spatial resolution given by the subwavelength extent of the cavity mode, which can be below 40 nm in 2D PPC shift cavity modes.[35]

■ ASSOCIATED CONTENT

Supporting Information

Fabrications of PPC cavities, coupled graphene-cavity model, and characterization of the cavity used to enhance graphene Raman scattering. This material is available free of charge via the Internet at http://pubs.acs.org/.

■ AUTHOR INFORMATION

Corresponding Author

*E-mail: englund@columbia.edu.

Notes

The authors declare no competing financial interest.

■ ACKNOWLEDGMENTS

The authors thank Kangmook Lim for the cavity etching and Arend van der Zande for the helpful discussions. Financial support was provided by the Air Force Office of Scientific Research PECASE, supervised by Dr. Gernot Pomrenke, and MURI programs, by the DARPA Information in a Photon program, through Grant No. W911NF-10-1-0416, and by the National Science Foundation through grant DMR-1106225. Fabrication of the PPC was carried out at the Center for Functional Nanomaterials, Brookhaven National Laboratory, which is supported by the U.S. Department of Energy, Office of Basic Energy Sciences, under Contract No. DE-AC02-98CH10886. Device assembly, including graphene transfer, and characterization was supported by the Center for Re-Defining Photovoltaic Efficiency Through Molecule Scale Control, an Energy Frontier Research Center funded by the U.S. Department of Energy, Office of Science, Office of Basic Energy Sciences under Award Number DE-SC0001085.

■ REFERENCES

(1) Bonaccorso, F.; Sun, Z.; Hasan, T.; Ferrari, A. C. *Nat. Photonics* **2010**, *4*, 611−622.
(2) Konstantatos, G.; Badioli, M.; Gaudreau, L.; Osmond, J.; Bernechea, M.; de Arquer, F. P. G.; Gatti, F.; Koppens, F. H. L. *Nat. Nanotechnol.* **2012**, *7*, 363−368.
(3) Mueller, T.; Xia, F.; Avouris, P. *Nat. Photonics* **2010**, *4*, 297−301.
(4) Xia, F.; Mueller, T.; Lin, Y.-M.; Valdes-Garcia, A.; Avouris, P. *Nat. Nanotechnol.* **2009**, *4*, 839−43.
(5) Lemme, M. C.; Koppens, F. H. L.; Falk, A. L.; Rudner, M. S.; Park, H.; Levitov, L. S.; Marcus, C. M. *Nano Lett.* **2011**, *11*, 4134−7.
(6) Liu, M.; Yin, X.; Ulin-Avila, E.; Geng, B.; Zentgraf, T.; Ju, L.; Wang, F.; Zhang, X. *Nature* **2011**, *474*, 64−7.
(7) Liu, M.; Yin, X.; Zhang, X. *Nano Lett.* **2012**, *12*, 1482−5.
(8) Bao, Q.; Zhang, H.; Wang, Y.; Ni, Z.; Yan, Y.; Shen, Z. X.; Loh, K. P.; Tang, D. Y. *Adv. Funct. Mater.* **2009**, *19*, 3077−3083.
(9) Sun, Z.; Hasan, T.; Torrisi, F.; Popa, D.; Privitera, G.; Wang, F.; Bonaccorso, F.; Basko, D. M.; Ferrari, A. C. *ACS Nano* **2010**, *4*, 803−810.
(10) Hendry, E.; Hale, P.; Moger, J.; Savchenko, A.; Mikhailov, S. *Phys. Rev. Lett.* **2010**, *105*, 097401.
(11) Zhang, Z.; Voss, P. L. *Opt. Lett.* **2011**, *36*, 4569−4571.
(12) Gu, T.; Petrone, N.; Mcmillan, J. F.; Zande, A. V. D.; Yu, M.; Lo, G. Q.; Kwong, D. L.; Hone, J.; Wong, C. W. *Nat. Photonics* **2012**, *43*, 1−6.
(13) Nair, R. R.; Blake, P.; Grigorenko, A. N.; Novoselov, K. S.; Booth, T. J.; Stauber, T.; Peres, N. M. R.; Geim, A. K. *Science* **2008**, *320*, 1308.
(14) Mak, K. F.; Sfeir, M. Y.; Wu, Y.; Lui, C. H.; Misewich, J.; Heinz, T. F. *Phys. Rev. Lett.* **2008**, *101*, 196405.
(15) Ju, L.; Geng, B.; Horng, J.; Girit, C.; Martin, M.; Hao, Z.; Bechtel, H. A.; Liang, X.; Zettl, A.; Shen, Y. R.; Wang, F. *Nat. Nanotechnol.* **2011**, *6*, 630−4.
(16) Koppens, F. H. L.; Chang, D. E.; Abajo, F. J. G. D. *Nano Lett.* **2011**, *11*, 3370−3377.
(17) Echtermeyer, T. J.; Britnell, L.; Jasnos, P. K.; Lombardo, A.; Gorbachev, R. V.; Grigorenko, A. N.; Geim, A. K.; Ferrari, A. C.; Novoselov, K. S. *Nat. Commun.* **2011**, *2*, 458.
(18) Liu, Y.; Cheng, R.; Liao, L.; Zhou, H.; Bai, J.; Liu, G.; Liu, L.; Huang, Y.; Duan, X. *Nat. Commun.* **2011**, *2*, 579.
(19) Chen, J.; Badioli, M.; Alonso-González, P.; Thongrattanasiri, S.; Huth, F.; Osmond, J.; Spasenovíc, M.; Centeno, A.; Pesquera, A.; Godignon, P.; Elorza, A. Z.; Camara, N.; García de Abajo, F. J.; Hillenbrand, R.; Koppens, F. H. L. *Nature* **2012**, *487*, 77−81.
(20) Fei, Z.; Rodin, A. S.; Andreev, G. O.; Bao, W.; McLeod, A. S.; Wagner, M.; Zhang, L. M.; Zhao, Z.; Thiemens, M.; Dominguez, G.; Fogler, M. M.; Castro Neto, A. H.; Lau, C. N.; Keilmann, F.; Basov, D. N. *Nature* **2012**, *487*, 82−5.

(21) Furchi, M.; Urich, A.; Pospischil, A.; Lilley, G.; Unterrainer, K.; Detz, H.; Klang, P.; Andrews, A. M.; Schrenk, W.; Strasser, G.; Mueller, T. *Nano Lett.* **2012**, *12*, 2773−7.
(22) Akahane, Y.; Asano, T.; Song, B.-S.; Noda, S. *Nature* **2003**, *425*, 944−947.
(23) Dean, C. R.; Young, A. F.; Meric, I.; Lee, C.; Wang, L.; Sorgenfrei, S.; Watanabe, K.; Taniguchi, T.; Kim, P.; Shepard, K. L.; Hone, J. *Nat. Nanotechnol.* **2010**, *5*, 722−6.
(24) Suk, J. W.; Kitt, A.; Magnuson, C. W.; Hao, Y.; Ahmed, S.; An, J.; Swan, A. K.; Goldberg, B. B.; Ruoff, R. S. *ACS Nano* **2011**, *5*, 6916−24.
(25) Englund, D.; Faraon, A.; Fushman, I.; Stoltz, N.; Petroff, P.; Vuckovic, J. *Nature* **2007**, *450*, 857−861.
(26) Lacey, S. D. *Solid State Commun.* **1970**, *8*, 1115−1118.
(27) Kravets, V. G.; Grigorenko, A. N.; Nair, R. R.; Blake, P.; Anissimova, S.; Novoselov, K. S.; Geim, A. K. *Phys. Rev. B* **2010**, *81*, 155413.
(28) Joannapolous, J. D.; Johnson, S. G.; Winn, J. N.; Meade, R. D. *Photonic Crystals: Molding the Flow of Light*; Princeton University Press: Princeton, NJ, 2008.
(29) Akahane, Y.; Asano, T.; Song, B.-S.; Noda, S. *Opt. Express* **2005**, *13*, 1202−1214.
(30) Srinivasan, K.; Barclay, P.; Borselli, M.; Painter, O. *Phys. Rev. B* **2004**, *70*, 081306.
(31) Das, A.; Pisana, S.; Chakraborty, B.; Piscanec, S.; Saha, S. K.; Waghmare, U. V.; Novoselov, K. S.; Krishnamurthy, H. R.; Geim, A. K.; Ferrari, A. C.; Sood, A. K. *Nat. Nanotechnol.* **2008**, *3*, 210−5.
(32) Yoon, D.; Moon, H.; Son, Y.-W.; Park, B. H.; Kim, J. B.; Lee, Y.; Cheong, H. *Nano Lett.* **2008**, *8*, 4270−4.
(33) Manolatou, C.; Khan, M. J.; Fan, S.; Villeneuve, P. R.; Haus, H. A.; Fellow, L.; Joannopoulos, J. D. *IEEE J. Quantum Electron.* **1999**, *35*, 1322−1331.
(34) Begliarbekov, M.; Sul, O.; Santanello, J.; Ai, N.; Zhang, X.; Yang, E.-H.; Strauf, S. *Nano Lett.* **2011**, *11*, 1254−8.
(35) Kita, S.; Nozaki, K.; Baba, T. *Opt. Express* **2008**, *16*, 8174−80.